Development (2014) 141, 2260-2270 doi:10.1242/dev.103705

Shum, A. S. W., Poon, L. L. M., Tang, W. W. T., Koide, T., Chan, B. W. H., Leung, Y.-C. G., Shiroishi, T. and Copp, A. J. (1999). Retinoic acid induces down-regulation of Wnt-3a, apoptosis and diversion of tail bud cells to a neural fate in the mouse embryo. *Mech. Dev.* **84**, 17-30.

Sive, H. L., Draper, B. W., Harland, R. M. and Weintraub, H. (1990). Identification of a retinoic acid-sensitive period during primary axis formation in Xenopus laevis. *Genes Dev.* **4**, 932-942.

Sucov, H. M., Murakami, K. K. and Evans, R. M. (1990). Characterization of an autoregulated response element in the mouse retinoic acid receptor type beta gene. *Proc. Natl. Acad. Sci. U.S.A.* **87**, 5392-5396.

Takemoto, T., Uchikawa, M., Yoshida, M., Bell, D. M., Lovell-Badge, R., Papaioannou, V. E. and Kondoh, H. (2011). Tbx6-dependent Sox2 regulation determines neural or mesodermal fate in axial stem cells. *Nature* **470**, 394-398.

Tam, P. P. L., Goldman, D., Camus, A. and Schoenwolf, G. C. (2000). 1 Early events of somitogenesis in higher vertebrates: allocation of precursor cells during gastrulation and the organization of a meristic pattern in the paraxial mesoderm. *Curr. Top. Dev. Biol.* **47**, 1-32.

Thacher, S. M., Vasudevan, J. and Chandraratna, R. A. S. (2000). Therapeutic applications for ligands of retinoid receptors. *Curr. Pharm. Des.* **6**, 25-58.

Tsang, K. Y., Sinha, S., Liu, X., Bhat, S. and Chandraratna, R., A. (2003). Disubstituted Chalcone Oximes Having Rar(Gamma)-Retinoid Receptor Antagonist Activity. European Patent Office.

Uchiyama, H., Kobayashi, T., Yamashita, A., Ohno, S. and Yabe, S. (2001). Cloning and characterization of the T-box gene Tbx6 in Xenopus laevis. *Dev. Growth Differ.* **43**, 657-669.

von Dassow, G., Schmidt, J. E. and Kimelman, D. (1993). Induction of the Xenopus organizer: expression and regulation of Xnot, a novel FGF and activin-regulated homeo box gene. *Genes Dev.* **7**, 355-366.

Wellik, D. M. (2007). Hox patterning of the vertebrate axial skeleton. *Dev. Dyn.* **236**, 2454-2463.

Weston, A. D., Blumberg, B. and Underhill, T. M. (2003). Active repression by unliganded retinoid receptors in development: less is sometimes more. *J. Cell Biol.* **161**, 223-228.

Wong, C. W. and Privalsky, M. L. (1998). Transcriptional silencing is defined by isoform- and heterodimer-specific interactions between nuclear hormone receptors and corepressors. *Mol. Cell. Biol.* **18**, 5724-5733.

Yabe, T. and Takada, S. (2012). Mesogenin causes embryonic mesoderm progenitors to differentiate during development of zebrafish tail somites. *Dev. Biol.* **370**, 213-222.

Yoon, J. K. and Wold, B. (2000). The bHLH regulator pMesogenin1 is required for maturation and segmentation of paraxial mesoderm. *Genes Dev.* **14**, 3204-3214.

Yoon, J. K., Moon, R. T. and Wold, B. (2000). The bHLH class protein pMesogenin1 can specify paraxial mesoderm phenotypes. *Dev. Biol.* **222**, 376-391.

Young, T., Rowland, J. E., van de Ven, C., Bialecka, M., Novoa, A., Carapuco, M., van Nes, J., de Graaff, W., Duluc, I., Freund, J.-N. et al. (2009). Cdx and Hox genes differentially regulate posterior axial growth in mammalian embryos. *Dev. Cell* **17**, 516-526.

Genomics Data 2 (2014) 296–298

Contents lists available at ScienceDirect

Genomics Data

journal homepage: http://www.journals.elsevier.com/genomics-data/

Data in Brief

Gene expression response to EWS–FLI1 in mouse embryonic cartilage

Miwa Tanaka [a], Ken-ichi Aisaki [b], Satoshi Kitajima [b], Katsuhide Igarashi [b], Jun Kanno [b], Takuro Nakamura [a,*]

[a] Division of Carcinogenesis, The Cancer Institute, Japanese Foundation for Cancer Research, Tokyo, Japan
[b] Division of Cellular and Molecular Toxicology, Biosafety Research Center, National Institute of Health Science, Tokyo, Japan

ARTICLE INFO

Article history:
Received 21 August 2014
Received in revised form 3 September 2014
Accepted 7 September 2014
Available online 16 September 2014

Keywords:
cDNA microarrays
Embryonic cartilage
EWS–FLI1
Ewing's sarcoma
Gene expression profiling

ABSTRACT

Ewing's sarcoma is a rare bone tumor that affects children and adolescents. We have recently succeeded to induce Ewing's sarcoma-like small round cell tumor in mice by expression of EWS–ETS fusion genes in murine embryonic osteochondrogenic progenitors. The Ewing's sarcoma precursors are enriched in embryonic superficial zone (eSZ) cells of long bone. To get insights into the mechanisms of Ewing's sarcoma development, gene expression profiles between EWS–FLI1-sensitive eSZ cells and EWS–FLI1-resistant embryonic growth plate (eGP) cells were compared using DNA microarrays. Gene expression of eSZ and eGP cells (total, 30 samples) was evaluated with or without *EWS–FLI1* expression 0, 8 or 48 h after gene transduction. Our data provide useful information for gene expression responses to fusion oncogenes in human sarcoma.

Specifications	
Organism/cell line/tissue	*Mus musculus*
Strain	BALB/c, dpc 18.5
Sex	Both male and female
Array type	Affymetrix MOE430 2.0 array
Data format	Raw data: CEL files, processed data: Excel table
Experimental factors	Tissue
Experimental features	Gene expression in eSZ cells and eGP cells with or without EWS–FLI1 expression was compared
Consent	n/a

Direct link to deposited data

Deposited data can be found here: http://www.ncbi.nlm.nih.gov/geo/query/acc.cgi?acc=GSE32618.

Experimental design, materials and methods

Preparation of mouse embryonic superficial zone (eSZ) and growth plate (eGP) cells

Femoral and humeral bones of BALB/c mouse embryos were removed aseptically on 18.5 dpc, and they were microdissected into eSZ and growth plate (eGP) under a stereomicroscope (Zeiss Stemi 2000-C, Carl Zeiss MicroImaging). Each region was minced and gently digested with 2 mg/mL of collagenase (Wako Pure Chemical) at 37 °C for 2 h. They were cultured in growth medium composed of Iscove's Modified Dulbecco's Medium (Invitrogen) supplemented with 15% fetal bovine serum, and subjected immediately to retroviral infection.

Retroviral infection

N-terminal FLAG-tagged *EWS–FLI1* was introduced into the pMYs-IRES-GFP vector. The full length *EWS–FLI1* cDNA was a kind gift from Dr. Susanne Baker. Retroviral infections of eSZ, eGP or shaft cells were performed as described [1]. Infection efficiency was examined using a FACSCalibur flow cytometer (Beckton Dickinson). Cells were harvested after fourty-eight hours of infection.

RNA isolation and microarray

GeneChip analysis was conducted to determine gene expression profiles. The per cell normalization method (Percellome method) was applied to eSZ and eGP samples [2]. Briefly, cellular lysates were prepared with RLT buffer (QIAGEN). A 10 μL aliquot of each lysate was treated with DNAse-free RNase A (Nippon Gene Inc., Japan) for 30 min at 37 °C, followed by Proteinase K (Roche Diagnostics GmbH., Germany) for 3 h at 55 °C. The aliquot was then transferred to a 96-well black plate. PicoGreen fluorescent dye (Molecular Probes Inc., USA) was added to each well, shaken for 10 s four times and then incubated for 2 min at 30 °C. DNA concentration was measured using a 96

* Corresponding author. Tel.: + 81 335700462.
E-mail address: takuro-ind@umin.net (T. Nakamura).

http://dx.doi.org/10.1016/j.gdata.2014.09.003

well fluorescence plate reader with excitation at 485 nm and emission at 538 nm. λ phage DNA (PicoGreen Kit, Molecular Probes Inc., USA) was used as standard. As reported previously [2], the grade-dosed spike cocktails (GSCs) made of the *Bacillus subtilis* RNAs corresponding to the sequences in the Affymetrix GeneChip arrays (AFFX-ThrX-3_at, AFFX-LysX-3_at, AFFX-PheX-3_at, AFFX-DapX-3_at, and AFFX-TrpnX-3_at) were prepared, and GSCs were added to the sample homogenates in proportion to their DNA concentrations. Total RNA was extracted using the RNeasy Mini Kit (QIAGEN). The GeneChip Mouse Genome 430 2.0 Array (Affymetrix) was hybridized with the cRNA generated from eSZ and eGP cells, and murine Ewing's sarcoma tissue (Table 1). After staining with streptavidin–phycoerythrin conjugates, arrays were scanned using an Affymetrix GeneChip Scanner 3000 and analyzed using Affymetrix GeneChip Command Console Software (AGCC, Affymetrix) and GeneSpring GX 11.0.2 (Agilent Technologies) as described previously [3]. The expression data for eSZ and eGP cells were converted to Percellome data, i.e., absolute copy numbers of mRNA per one cell, by the homemade software SCal4 (Spike Calculation version 4). This software also graphically indicates the efficiency of in vitro transcription, the dose–response linearity of the five GSC spikes and the location of spike probe sets in the histogram of all probe sets (Fig. 1A). From the same treatment group (n = 3), all the pairs were plotted to a scatter graph as red (expression above detection level) or green dots (below detection level) with the data of five yellow spike probe sets (Fig. 1B). If any samples did not draw a symmetric scatter plot with yellow dot on the diagonal line, the sample were rejected for evaluation, and they were subjected to additional analyses.

Data analysis

Homemade software named RSort (Roughness Sort) [4] was used. This program sorts the probe sets as upward or downward peaks in a 3D isobologram (Fig. 2). To avoid biologically nonsense probe sets

Table 1
Summary of processed samples.

GEO accession no.	Cell types	Gene transfer	Time (h)
GSM808581	eSZ	No	0
GSM808582	eSZ	No	0
GSM808583	eSZ	No	0
GSM808584	eGP	No	0
GSM808585	eGP	No	0
GSM808586	eGP	No	0
GSM808587	eSZ	Empty vector	8
GSM808588	eSZ	Empty vector	8
GSM808589	eSZ	Empty vector	8
GSM808590	eGP	Empty vector	8
GSM808591	eGP	Empty vector	8
GSM808592	eGP	Empty vector	8
GSM808593	eSZ	EWS–FLI1	8
GSM808594	eSZ	EWS–FLI1	8
GSM808595	eSZ	EWS–FLI1	8
GSM808596	eGP	EWS–FLI1	8
GSM808597	eGP	EWS–FLI1	8
GSM808598	eGP	EWS–FLI1	8
GSM808599	eSZ	Empty vector	48
GSM808600	eSZ	Empty vector	48
GSM808601	eSZ	Empty vector	48
GSM808602	eGP	Empty vector	48
GSM808603	eGP	Empty vector	48
GSM808604	eGP	Empty vector	48
GSM808605	eSZ	EWS–FLI1	48
GSM808606	eSZ	EWS–FLI1	48
GSM808607	eSZ	EWS–FLI1	48
GSM808608	eGP	EWS–FLI1	48
GSM808609	eGP	EWS–FLI1	48
GSM808610	eGP	EWS–FLI1	48

eSZ, embryonic superficial zone; GP, growth plate.

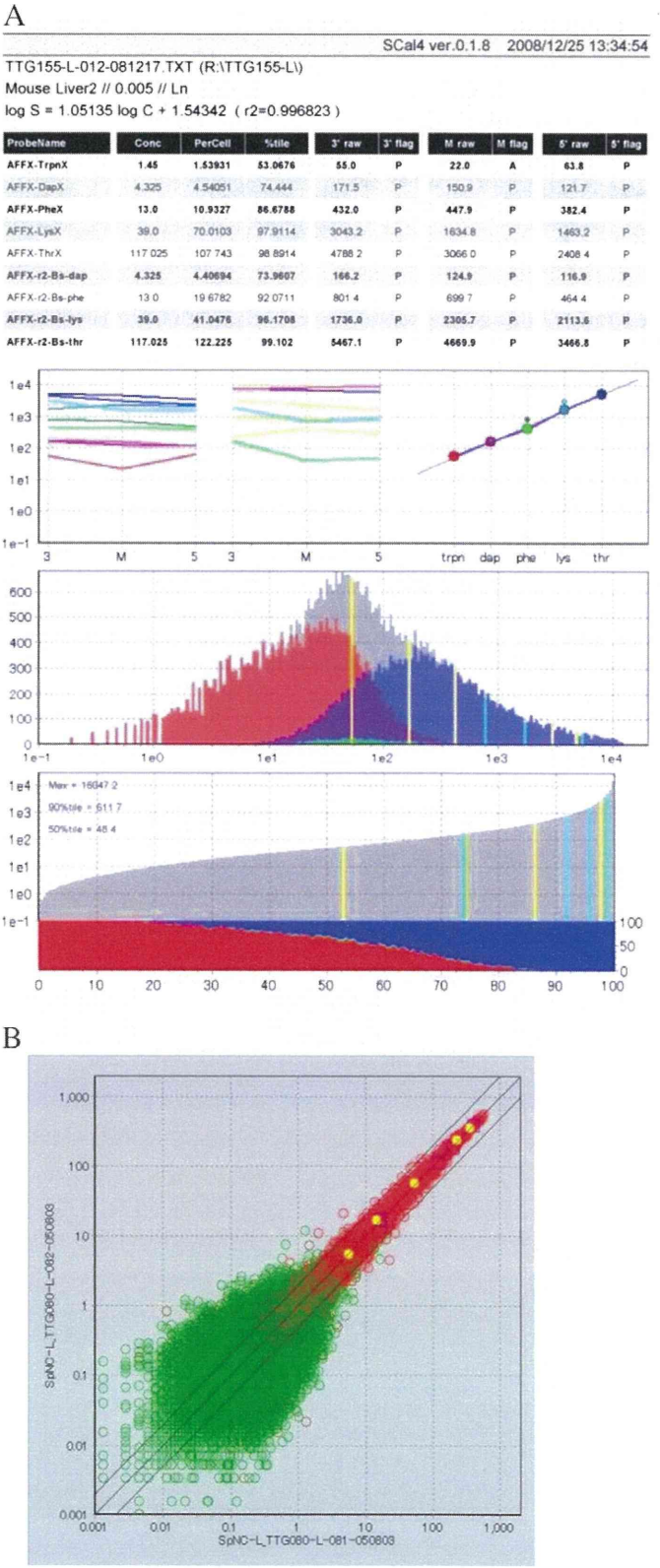

Fig. 1. Evaluation of the microarray data according to the PerCellome method. (A) An example of the SCal4 software report. SCal4 graphically indicates the efficiency of in vitro transcription, the dose–response linearity of the five GSC spikes and the location of spike probe sets in the histogram of all probe sets. (B) A scatter plot of gene expression between two experimental groups. All the pairs of probe sets were plotted to a scatter graph as red (expression above detection level) or green dots (below detection level) with the data of five yellow spike probe sets.

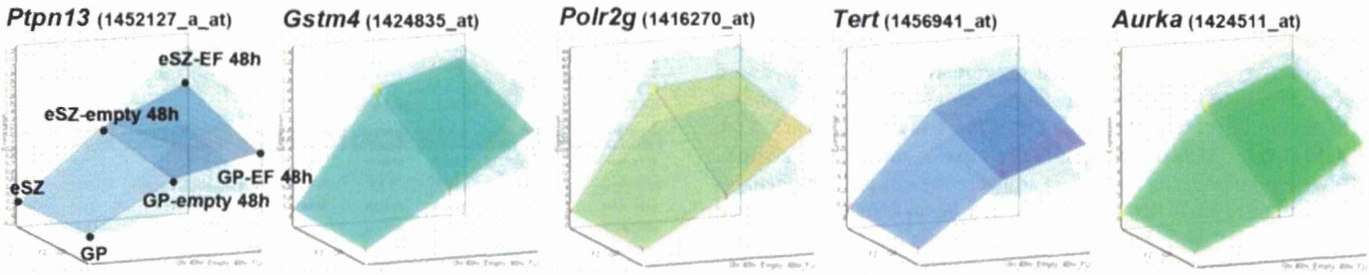

Fig. 2. Modulation of gene expression following introduction of *EWS–FLI1*. Three-dimensional grid plots of the expression of five representative genes in eSZ and eGP cells with or without *EWS–FLI1* were generated by GeneChip analysis (first two rows). The averages of each group ($n = 3$) were calculated and plotted as three layers of isobolograms on three-dimensional graphs as described previously [2,4].

such as ones with expression below the detection level, the data were visually checked for their 3D isobologram shape.

Discussion

We describe a unique dataset of mouse embryonic cartilage with or without the Ewing's sarcoma fusion oncogene, *EWS–FLI1*. Significantly different responses of gene expression between eSZ and eGP cells were observed. The dataset was used in the study published recently [5] and was informative to understand the tumorigenic mechanisms of Ewing's sarcoma.

References

[1] G. Jin, et al., Trib1 and Evi1 cooperate with Hoxa and Meis1 in myeloid leukemogenesis. Blood 109 (9) (2007) 3998–4005.
[2] J. Kanno, et al., "Per cell" normalization method for mRNA measurement by quantitative PCR and microarrays. BMC Genomics 7 (2006) 64.
[3] T. Fujino, et al., Function of EWS-POU5F1 in sarcomagenesis and tumor cell maintenance. Am. J. Pathol. 176 (4) (2010) 1973–1982.
[4] J. Kanno, et al., Oral administration of pentachlorophenol induces interferon signaling mRNAs in C57BL/6 male mouse liver. J. Toxicol. Sci. 38 (4) (2013) 643–654.
[5] M. Tanaka, et al., Ewing's sarcoma precursors are highly enriched in embryonic osteochondrogenic progenitors. J. Clin. Invest. 124 (7) (2014) 3061–3074.

Ewing's sarcoma precursors are highly enriched in embryonic osteochondrogenic progenitors

Miwa Tanaka,[1] Yukari Yamazaki,[1] Yohei Kanno,[1] Katsuhide Igarashi,[2] Ken-ichi Aisaki,[2] Jun Kanno,[2] and Takuro Nakamura[1]

[1]Division of Carcinogenesis, The Cancer Institute, Japanese Foundation for Cancer Research, Tokyo, Japan.
[2]Division of Cellular and Molecular Toxicology, Biosafety Research Center, National Institute of Health Science, Tokyo, Japan.

Ewing's sarcoma is a highly malignant bone tumor found in children and adolescents, and the origin of this malignancy is not well understood. Here, we introduced a Ewing's sarcoma–associated genetic fusion of the genes encoding the RNA-binding protein EWS and the transcription factor ETS (*EWS-ETS*) into a fraction of cells enriched for osteochondrogenic progenitors derived from the embryonic superficial zone (eSZ) of long bones collected from late gestational murine embryos. *EWS-ETS* fusions efficiently induced Ewing's sarcoma–like small round cell sarcoma formation by these cells. Analysis of the eSZ revealed a fraction of a precursor cells that express growth/differentiation factor 5 (*Gdf5*), the transcription factor *Erg*, and parathyroid hormone-like hormone (*Pthlh*), and selection of the *Pthlh*-positive fraction alone further enhanced *EWS-ETS*–dependent tumor induction. Genes downstream of the EWS-ETS fusion protein were quite transcriptionally active in eSZ cells, especially in regions in which the chromatin structure of the ETS-responsive locus was open. Inhibition of β-catenin, poly (ADP-ribose) polymerase 1 (PARP1), or enhancer of zeste homolog 2 (EZH2) suppressed cell growth in a murine model of Ewing's sarcoma, suggesting the utility of the current system as a preclinical model. These results indicate that eSZ cells are highly enriched in precursors to Ewing's sarcoma and provide clues to the histogenesis of Ewing's sarcoma in bone.

Introduction

Ewing's sarcoma is a highly malignant bone tumor in children and adolescents. It frequently develops as a small round cell sarcoma in the metaphysis of long bones (1). The origin of Ewing's sarcoma has been an enigma since the first case was reported in 1921 (2). Primitive neural crest cells, hematopoietic cells, and muscle cells as well as mesenchymal stem cells (MSCs) have been considered possible cells of origin (3, 4). Chromosomal translocation-related genetic fusions between *EWSR1* on chromosome 22 and genes encoding ETS family transcription factors, such as *FLI1* and *ERG*, were then identified. The EWS and the transcription factor ETS (*EWS-ETS*) fusion is now considered a genetic hallmark of human Ewing's sarcoma (5–7). However, it has been difficult to establish an appropriate animal model by introduction of *EWS-ETS* chimeras (8), suggesting that introduction of *EWS-ETS* is not sufficient to define the origin of the tumors. A few groups have reported successful development of Ewing's sarcoma–like tumors by introduction of *EWS-FLI1* into murine mesenchymal cells (9, 10). However, it is unclear whether there is a special subfraction that includes the cell of origin of Ewing's sarcoma. The difficulty of inducing Ewing's sarcoma suggests that the target cells of *EWS-ETS* might be the cells of a narrow lineage and/or of a limited differentiation stage.

Unlike osteosarcoma, which generally involves the metaphyses of long tubular bones, Ewing's sarcoma occurs at almost equal frequencies in flat bones and the diaphysis of tubular bones (11). This fact suggests that mutations related to the proliferation of bony tissue might not contribute to the genesis of Ewing's sarcoma. Moreover, it suggests that the primary genetic event, the EWS-ETS fusion, might occur at an earlier stage of bone development.

Members of the *ETS* family of genes that are involved in *EWS* fusions are important for transcriptional regulation in mouse embryonic and perinatal limb skeletogenesis (12). Accumulation of *Erg*$^+$ progenitor cells occurs in the embryonic superficial zone (eSZ) of long bones from dpc 15.5 to P7, after which expression is downregulated rapidly (13, 14). These results suggest that temporospatial expression of *Erg* might be critical for induction of bipotential progenitors during osteochondrogenic differentiation and that dysregulated expression due to chromosomal translocation and fusion to *EWSR1* might result in abnormal accumulation of progenitor cells that exhibit increased proliferative potency (10).

To clarify the possible cellular origin of Ewing's sarcoma, we purified eSZ cells from murine embryonic long bones that expressed *Erg* and introduced *EWS-FLI1* or *EWS-ERG* fusion genes. We found that EWS-ETS target cells were highly enriched in the eSZ fraction. Moreover, the epigenetic status of genes responsive to transcriptional regulation by EWS-ETS is important for Ewing's sarcoma development and its phenotypic manifestation.

Results

Development of Ewing's sarcoma–like small round cell tumors by EWS-ETS expression in the eSZ cells. *Erg*, one of the *EWS* fusion partners in Ewing's sarcoma, is transiently expressed in the joint surface of embryonic and perinatal bones. Therefore, we predicted that the *EWS-ETS* fusion would affect differentiation and induce abnormal proliferation of *Erg*-expressing cells. To test this hypothesis, femoral and humeral bones of dpc 18.5 murine embryos were separated into the eSZ, embryonic growth plate (eGP), the embryonic shaft and synovial regions (eSyR) by microdissection (Figure 1A). Embryonic mesenchymal cells of the head and trunk were also prepared. Each cell fraction was mildly digested with type I collagenase. The cells were immediately subjected to retrovirus-mediated

Conflict of interest: The authors have declared that no conflict of interest exists.
Citation for this article: *J Clin Invest.* 2014;124(7):3061–3074. doi:10.1172/JCI72399.

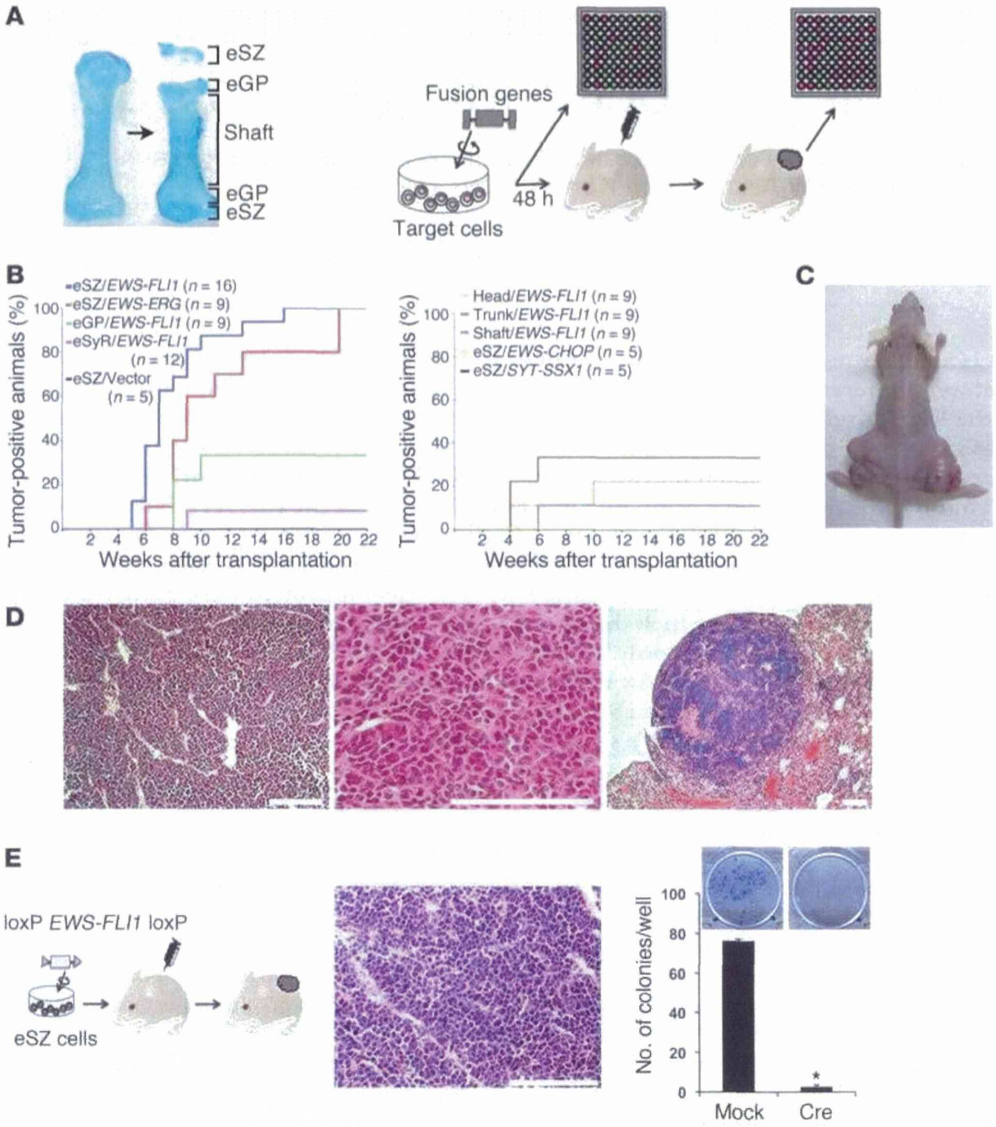

Figure 1

Development of murine Ewing's sarcoma. (**A**) Microdissection of mouse embryonic bone. The femur was lightly stained with methylene blue. Experimental strategy of the ex vivo model. Each cell type targeted with *EWS-ETS* was injected into nude mice or subjected to gene expression profiling. (**B**) Cumulative incidence (percentage) of small round cell tumors induced by eSZ, eGP, and eSyR cells expressing *EWS-ETS* or by eSZ with an empty vector and by embryonic mesenchymal cells of the trunk, head, and shaft expressing *EWS-FLI1* or eSZ expressing *EWS-CHOP* or *SYT-SSX1*. $P < 0.02$ in eSZ/*EWS-FLI1* vs. eGP, eSyR, or shaft; $P < 0.04$ in eSZ/*EWS-FLI1* vs. trunk and head, log-rank test. (**C**) Tumors were observed as subcutaneous masses in recipient nude mice. (**D**) Histology of murine Ewing's sarcoma. H&E staining, with low (left) and high (center) magnification. Pulmonary metastasis of murine Ewing's sarcoma developed by tail vein injection of tumor cells (right). Scale bar: 100 μm. (**E**) Cre/*loxP*-mediated knockout of the *EWS-FLI1* transgene. Ewing's sarcoma developed by transplantation of eSZ cells transduced with the floxed *EWS-FLI1* retrovirus (left). Sarcoma cells were then maintained in vitro and transduced with the pMSCV-Cre retrovirus. Cre expression suppressed colony formation (right). The experiment was repeated 3 times and the representative results, are shown (graph inset). Scale bar: 100 μm. *$P < 0.01$. The mean ± SEM of 3 independent experiments is shown.

gene transfer of *EWS-FLI1* to all cell types by spin infection. The transduction efficiency was examined by flow cytometric analyses (Supplemental Figure 1A; supplemental material available online with this article; doi:10.1172/JCI72399DS1), and the expression of EWS-FLI1 was confirmed by FACS and immunofluorescent staining using anti-FLAG (Supplemental Figure 1, B–D). One million transduced cells of each fraction were injected subcutaneously into nude mice. Recipients transplanted with eSZ cells transduced with *EWS-FLI1* or *EWS-ERG* developed a subcutaneous mass at 100% penetrance, with a mean latency of 8 weeks (Figure 1, B–D).

As few as 1×10^4 injected transduced eSZ cells could develop Ewing's sarcomas. In contrast, 1×10^6 cells from *EWS-FLI1*–transduced eGP, embryonic shaft, or eSyR fractions were required for tumor development, clearly indicating that Ewing's sarcoma precursors were highly enriched in the eSZ fraction (Table 1). When embryonic mesenchymal cells purified from the mouse

Table 1
Summary of the incidences of tumors in limiting dilution experiments using eSyR, eSZ, eGP, shaft, trunk, or head cells

Cells	Numbers of transplanted cells		
	1×10^6	1×10^5	1×10^4
eSZ	25/25 (100%)	12/13 (92%)	4/5 (80%)
eGP	3/9 (33%)	0/7 (0%)	ND
eSyR	2/12 (17%)	0/10 (0%)	ND
Shaft	1/9 (11%)	0/6 (0%)	ND
Trunk	3/9 (33%)	1/10 (10%)	0/5 (0%)
Head	2/9 (22%)	1/7 (14%)	0/5 (0%)

ND, not done.

head or trunk were transduced with *EWS-FLI1*, the incidence of small round cell sarcomas was again lower, and fibrosarcoma-like tumors were also obtained (Figure 1B and Supplemental Figure 2A). In addition, no tumor was induced when *EWS-CHOP* or *SYT-SSX1*, which are found in myxoid liposarcoma or synovial sarcoma, respectively, were introduced into eSZ cells (Figure 1B). Development of nonneoplastic bone and cartilage was observed when we transplanted eSZ cells treated with an empty vector (Supplemental Figure 2B).

Histological analysis showed that tumors expressing *EWS-FLI1* or *EWS-ERG* were composed of aggressively growing, small round cells, a feature typical of Ewing's sarcoma (Figure 1D). All the tumors examined (10 of 10) were capable of secondary transplantation (Supplemental Table 1 and Supplemental Figure 2C), and 3 of 9 tumors had metastatic potential by tail vein injection (Figure 1D, Supplemental Table 1, and Supplemental Figure 2D). EWS-ETS expression was confirmed by immunoblotting and immunostaining of FLAG-tagged proteins (Supplemental Figure 2E). MIC2 (also known as CD99), a surface marker for human Ewing's sarcoma (15), was focally detected (Supplemental Figure 2F). *Cd99* gene sequences are only partially conserved between human and mouse (16), and therefore, CD99 was not useful as a specific marker for murine Ewing's sarcoma.

Cre/loxP-mediated genetic recombination and knockout of the *EWS-FLI1* transgene induced complete growth arrest of the tumor (Figure 1E), and senescence-like cellular phenotypes were observed in 91.4% of surviving cells (1.4% in non-Cre-treated cells) (Supplemental Figure 3). Thus, murine Ewing's sarcoma is dependent on *EWS-FLI1* activity. These results indicate that cellular targeting of eSZ cells by *EWS-ETS* fusion genes efficiently and specifically induced human Ewing's-like sarcoma in mice.

In addition, the monoclonal or oligoclonal nature of murine Ewing's sarcoma was indicated by cloning of retroviral integration sites (Supplemental Excel File 1). The tumors (n = 21) contained an average of 2.5 integration sites, and no common integration site has been identified, although there are interesting genes involved in neoplastic processes, such as *Ccnd3*, *Junb*, *Bach2*, and *Fyn*.

eSZ cells were characterized as osteochondrogenic progenitors. After condensation of mesenchymal stem/progenitor cells, the primitive structure of joint surfaces develops, and a chondrogenic progenitor lineage-rich eSZ emerges on the joint surface to develop the long bone from dpc 15.5 to P7 (Figure 2A and refs. 13, 17). eSZ cells purified by microdissection were positive for CD29 but lacked surface markers for MSC, such as SCA1, CD34, CD44, and CD105, in contrast to embryonic trunk cells (Supplemental Figure 4A). eSZ cells were also negative for Gr-1, FLK1, and CD45 (Supplemental Figure 4A and data not shown). These data indicated that eSZ cells constituted a different cohort from those making up the previously defined MPC fraction that is positive for CD44, Thy1 (CD90), and SCA1 (9).

We compared gene expression profiles of purified eSZ and eGP cells obtained by microdissection. The results suggested that eSZ cells were an immature chondrogenic precursor (Supplemental Table 2 and Supplemental Excel File 2). Furthermore, laser microdissection, followed by expression analyses of a series of differentiation-related genes, was carried out to assess the gene expression profile of the eSZ fraction (Figure 2, B–D). As expected, *Erg* and growth/differentiation factor 5 (*Gdf5*) expression was prominent in eSZ cells. Moreover, eSZ cells showed gene expression profiles characteristic of immature chondrogenic precursors, including parathyroid hormone-like hormone (*Pthlh*), *Prg4*, and *Col2a1*, consistent with previous studies (Figure 2C and refs. 12, 18, 19). On the other hand, eGP cells showed a more differentiated chondrocytic gene expression profile, as represented by *Col10a1* (Figure 2C). Also, *Nanog*, *Oct4*, and *Sox2* (together denoted as NOS), which are expressed in most immature lineages, were enriched in eSyR, whereas little or no expression was observed in eSZ or eGP fractions. The results are summarized in Table 2, and they indicate that enrichment of an $ERG^{hi}/GDF5^{hi}/PTHLH^{hi}/PRG4^{hi}/NOS^{lo}$ fraction was achieved by fine selection of eSZ cells. *Gdf5* was transiently expressed in eSZ cells and is a master regulator of joint formation (20). *Gdf5* promoter activity was also exhibited exclusively in eSZ cells (Supplemental Figure 4B).

In an in vitro differentiation assay, eSZ cells exhibited remarkable osteogenic and chondrogenic differentiation potencies but lacked the ability to differentiate into the adipogenic lineage. In contrast, embryonic mesenchymal progenitor cells showed their typical multilineage differentiation pattern (Figure 2D). Adipogenesis-related genes, such as *Pparg* and *Fabp4*, were not expressed in eSZ cells, but they were observed in eSyR cells (Supplemental Figure 4C). Also, eSZ cells were unable to differentiate into myogenic or neuronal lineages (Supplemental Figure 4D).

The tumor induction efficiency was further enhanced by immune selection of the eSZ cells using PTHLH (Supplemental Figure 1D), a marker that is expressed by periarticular cells and articular chondrocytes (17, 21, 22). All the recipients transplanted with 1×10^4 $PTHLH^+$ eSZ cells developed Ewing's sarcoma with a significantly shorter latency than that of those receiving unselected eSZ cells ($P < 0.01$). In contrast, no tumors were developed by recipients of the $PTHLH^-$ fraction of eSZ cells (Figure 2E; see complete unedited blots in the supplemental material). In addition, $PTHLH^+$ eSZ cells showed higher expression of *Erg* and *Gdf5* than the $PTHLH^-$ fraction (Figure 2F). These findings indicated that bipotential progenitors were present in the eSZ fraction and that successful enrichment of Erg^+ and $Pthlh^+$ progenitor cells was achieved in the eSZ cell fraction. eSZ cells were therefore used for the *EWS-ETS* gene transfer and subsequent transplantation experiments.

Early neoplastic lesions of murine Ewing's sarcoma. Our new animal model enabled us to examine how malignant cells progressed from preneoplastic and/or early neoplastic stages of cancer, stages that are difficult to observe in human Ewing's sarcoma (23). Early lesions of murine Ewing's sarcoma were therefore analyzed microscopically (Figure 3). Small foci of EWS-FLI1–positive (FLAG-positive) cells were observed adjacent to nonneoplastic cartilage (Figure 3A). Rapid cell cycle progression was confirmed in assess-

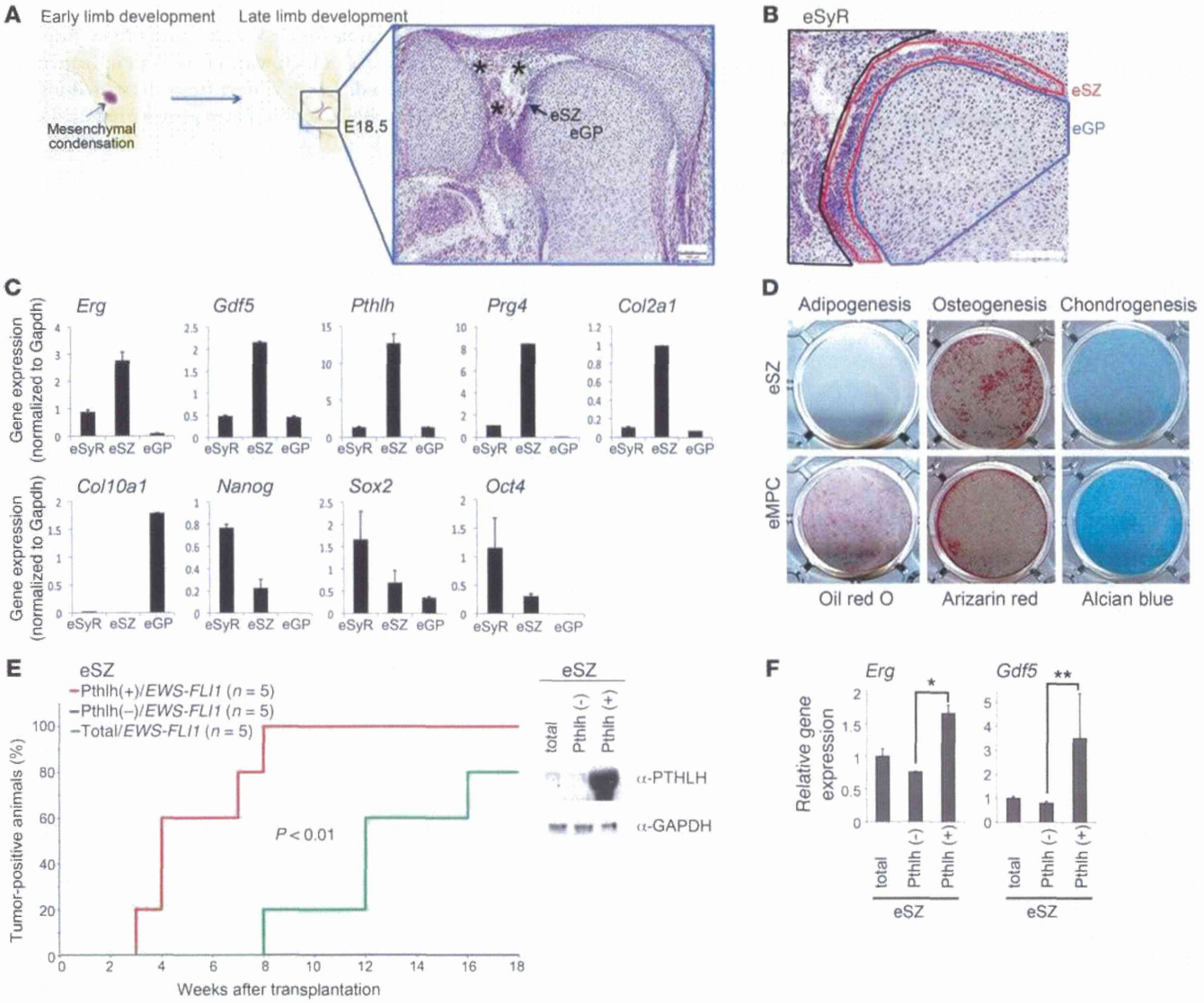

Figure 2

Characterization of eSZ cells. (**A**) Schematic illustration and histology of the developing knee joint in dpc 18.5 embryo. eSZ and eGP are indicated. Asterisks denote eSyR. Scale bar: 100 μm. (**B**) eSZ, eGP, and eSyR components were fractionated by laser microdissection and subjected to gene expression analysis. Scale bar: 100 μm. (**C**) Differentially expressed genes among eSyR, eSZ, and eGP cells. Quantitative RT-PCR analysis for *Erg*, *Gdf5*, *Pthlh*, *Prg4*, *Col2a1*, *Col10a1*, *Nanog*, *Sox2*, and *Oct4* expression in eSyR, eSZ, and eGP cells. The mean ± SEM of 3 independent experiments are shown. (**D**) In vitro differentiation assays of eSZ cells and trunk mesenchymal progenitor cells (eMPC). Adipogenic, osteogenic, and chondrogenic differentiation was induced in embryonic mesenchymal progenitor cells, whereas eSZ cells showed no adipogenic differentiation. The experiment was repeated 3 times, and representative results are shown. (**E**) PTHLH$^+$ and PTHLH$^-$ fractions were separated using biotinylated anti-PTHLH and avidin-conjugated magnetic beads. Tumor induction was examined by transplantation of each fraction (1×10^4 cells). $P < 0.01$ in PTHLH$^+$ eSZ/*EWS-FLI1* vs. total eSZ, log-rank test. Condensation of the PTHLH$^+$ fraction was confirmed by immunoblotting. (**F**) Expression of *Erg* and *Gdf5* in PTHLH$^+$ and PTHLH$^-$ eSZ cells. The mean ± SEM of 3 independent experiments are shown. $^*P < 0.01$; $^{**}P < 0.05$.

ments of BrdU incorporation (Figure 3B). The early neoplastic lesions did not express neural, myogenic, epithelial, vascular, or hematopoietic markers, including CD57, NGFR, S-100, myosin, desmin, von Willebrand factor, cytokeratin, or CD45 (data not shown). A few FLAG-positive cells expressed collagen type 2, a marker of immature chondrocytes (18, 24), and were observed in the peripheral areas around the early neoplastic foci (Figure 3C). Interestingly, these differentiating cells exhibited cytoplasmic staining for EWS-FLI1. Staining was essentially localized to the nucleus in the central part of the early neoplastic lesion (Figure 3B). Whereas nuclear localization of EWS-FLI1 fusion protein has been confirmed in most cell types (25), its cytoplasmic localization in differentiating cells suggests that cytoplasmic exclusion of EWS-FLI1 might represent an inhibitory mechanism in tumorigenesis of Ewing's sarcoma. The existence of cytoplasmic exclusion suggests that EWS-FLI1 expression alone is insufficient to induce complete tumorigenesis. In addition, more differentiated chondrocytes, positive for S100 or collagen type 10, were observed

Table 2
Summary of eSZ cell profiles

Gene	Expression properties	
	Levels in eSZ	Other mesenchymes
Erg	High	SZ (E)
Gdf5	High	SZ (E)
Pthlh	High	SZ (E, A)
Prg4	High	SZ (E, A)
Col2a1	Moderate	Proliferating chondrocytes (E, A)
Col10a1	None	Hypertrophic chondrocytes (E, A)
Nanog	Low	ES, EMPC
Sox2	low	ES, EMPC
Oct4	low	ES, EMPC

SZ, superficial zone or articular cartilage; ES, embryonic stem cell; EMPC, embryonic mesenchymal progenitor cell. Parenthetical E or A indicate embryo or adult, respectively.

in the surrounding area (Figure 3D and Supplemental Figure 5). EWS-FLI1 expression was hardly detected in S100-positive cells (Figure 3D). Microdissection and gene expression analyses of early neoplastic lesions revealed continued expression of *Erg*, *Gdf5*, *Pthlh*, and *Prg4*, whereas, in differentiated areas, downregulation of those genes was accompanied by increased *Col10a1* expression (Figure 3E). Those results indicated that the nature of the eSZ is preserved in the early neoplastic lesion, at least in part.

Murine Ewing's sarcoma shared common gene expression profiles with human small round cell tumor, including Ewing's sarcoma and neuroblastoma. Expression profiles of murine Ewing's sarcomas were compared with those of a series of human sarcomas, including Ewing's sarcoma, malignant fibrous histiocytoma, myxoid liposarcoma, synovial sarcoma, osteosarcoma, neuroblastoma, and chondrosarcoma. Hierarchical clustering using common gene sets between mice and humans (1,819 probes selected from 23,860 probe sets) showed that the murine Ewing's sarcoma was quite similar to the human Ewing's sarcoma and neuroblastoma (Figure 4A). The results suggested a relationship between the present model and human Ewing's sarcoma. Moreover, the neuroblastoma-like small round cell morphology could be induced from osteochondrogenic precursor cells by *EWS-FLI1* expression.

To better understand the nature of the small round tumor cells, the expression profile of mouse Ewing's sarcoma was again compared with that of human Ewing's sarcoma, poorly differentiated synovial sarcoma, neuroblastoma, and malignant lymphoma, and the profile of human Ewing's sarcoma was compared with that of mouse tumors (Figure 4B). Two thousands probe sets "specific" for each tumor that showed larger differences of expression relative to the rest of the tumor types were selected in both human and mouse tumor groups. Then, lists of the 2,000 probes were compared between mouse Ewing's sarcoma and each human tumor and between human Ewing's sarcoma and each mouse tumor, resulting in the selection of human and mouse Ewing's sarcoma as the closest counterparts to each another (Figure 4B), though the data were not statistically significant except for malignant lymphoma. Collectively, these data indicate that the expression profiles depend in part on the cell morphology of the small round cell tumor. It is notable that EWS-FLI1 expression in murine eSZ cells could induce human Ewing's sarcoma–like gene expression profiles.

Common upregulated genes in murine and human Ewing's sarcoma are presented in Supplemental Excel File 3 and Supplemental Figure 6A. The analysis revealed that 336 genes were upregulated in both murine and human Ewing's sarcomas, including known EWS-FLI1 targets such as *Dkk2*, *Prkcb1*, enhancer of zeste homolog 2 (*Ezh2*), *Id2*, *Nkx2.2*, *Nr0b1*, and *Ptpn13* (26–32). Furthermore, 6,014 genes, including EWS-FLI1 targets such as *Aurka*, *Gstm4*, *Tert*, *Tnc*, and *Upp1*, were upregulated in murine Ewing's sarcoma (Figure 4C, Supplemental Excel File 3, and refs. 33–37). These 5 genes were identified by EWS-FLI1 overexpression or silencing studies or by an immunohistochemical analysis that might cause exclusion of them as upregulated genes in human Ewing's sarcoma. Twenty-two out of thirty upregulated targets proposed by Ordonez et al. (8) were indeed upregulated in our model. In addition, 360 genes (including *Tgfbr2*) (38) were downregulated in both murine and human Ewing's sarcoma (Supplemental Figure 6A and Supplemental Excel File 4). These genes were potentially EWS-FLI1–responsive genes and might be important in the early oncogenic process as well as in the progression toward more malignant phenotypes. These gene expression results support the authenticity of our murine model for human Ewing's sarcoma.

The same analysis showed that 129 genes were upregulated in both murine and human Ewing's sarcoma as well as human neuroblastoma. Upregulation of a series of neuronal differentiation-related genes (*Gfra2*, *Ncan*, *Nrxn1*, and *Ntrk1*) and synapse-related genes (Supplemental Figure 6B) in murine Ewing's sarcoma was also observed in human neuroblastoma, indicating that the neuronal phenotype could be induced from osteochondrogenic progenitors, probably through transdifferentiation processes. The neuroectodermal-related signaling pathway, including NTRK1/NTRK3 and N-MYC, might play some role in neuronal phenotypes of Ewing's sarcoma. Although the number of commonly upregulated genes in murine Ewing's sarcoma and neuroblastoma was larger than that in murine and human Ewing's sarcoma, most of the known target genes described above were included in the latter category, suggesting that the core mechanisms of EWS-FLI1 transcriptional regulation might be preserved in our model.

EWS-FLI1–responsive genes and chromatin modification in eSZ cells. The relationship between the cell of origin of Ewing's sarcoma and *EWS-ETS* fusions is important, given the strict limitations on the origin of murine Ewing's sarcoma. Gene expression profiles were therefore compared between eSZ and eGP cells in the presence or absence of *EWS-FLI1* (Figure 5A and Supplemental Excel File 5) (data are available at NCBI Gene Expression Omnibus [GEO] with accession number GSE32618). Most of the known EWS-FLI1 target genes (8) were upregulated in eSZ cells following *EWS-FLI1* introduction (Supplemental Excel File 5). *EWS-FLI1* encodes an aberrant transcription factor (8, 30), and the response to it differed between eSZ and eGP cells (Figure 5B, Supplemental Figure 7, and Supplemental Excel File 6). The different gene responses in eSZ and eGP cell fractions were probably caused by differences in chromatin conditions at target loci. Histone modifications were therefore examined on representative genes, such as *Dkk2*, *Prkcb1*, and *Ezh2*. Histones H3K9/K14ac and H3K4me, which are activation marks for gene expression, were observed predominantly in eSZ cells as well as mouse Ewing's sarcoma cells, whereas histone H3K9me3 and H3K27me3, which are repressive marks, were observed predominantly in eGP cells (Figure 5C). These results strongly suggest that transcriptional activation of EWS-ETS target genes occurred in eSZ cells at maximum efficiency and that

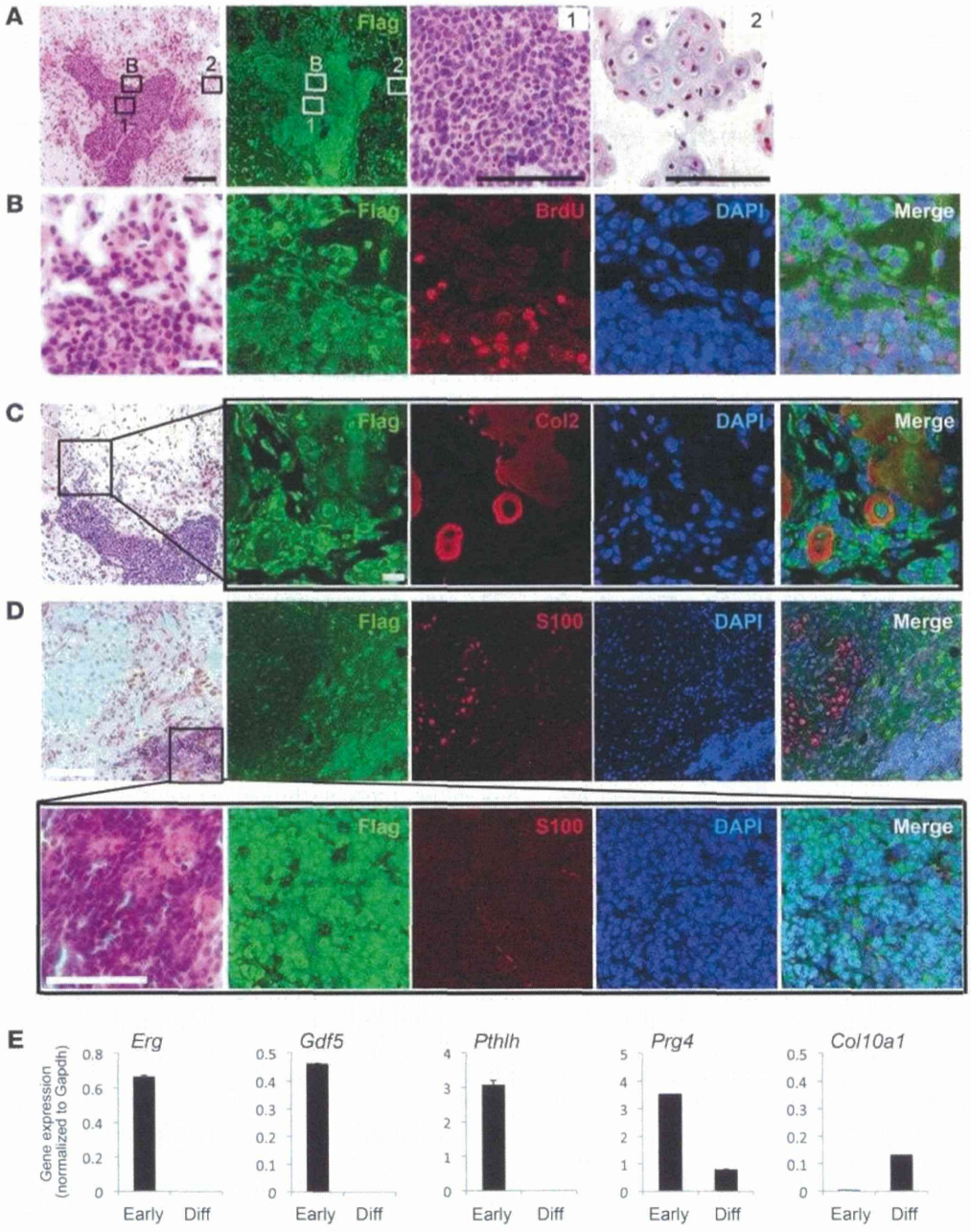

Figure 3

An early neoplastic lesion of murine Ewing's sarcoma 3 weeks after transplantation. (**A** and **B**) Immunofluorescent assessment of FLAG. (**A**) High-power images of early neoplastic cells (see boxed region 1 shown at higher magnification) and nonneoplastic cartilage (see boxed region 2 shown at higher magnification) are shown. Scale bar: 100 μm. (**B**) The boxed region in **A** shown at higher magnification. Accumulation of BrdU-positive nuclei in the central early neoplastic lesions. Nuclear localization of EWS-FLI1 (FLAG) was observed in the central region, whereas cytoplasmic translocation of EWS-FLI1 is remarkable in the differentiating zone. Scale bar: 20 μm. (**C**) The differentiating zone with cytoplasmic EWS-FLI1 staining is characterized by collagen 2 expression. Scale bar: 20 μm. (**D**) Further differentiation toward the chondrogenic lineage in a more peripheral area is indicated by expression of S100 (top row), which is negative in the central early neoplastic lesion (bottom row). Scale bar: 100 μm. (**E**) Quantitative real-time PCR analysis for *Erg*, *Gdf5*, *Pthlh*, *Prg4*, and *Col10a1* expression in early neoplastic cells and the differentiating zone. The mean ± SEM of 3 independent experiments are shown.

the histone status in eSZ cells was preserved after transformation, thereby providing the aggressive oncogenic function of EWS-ETS.

Upregulation of the WNT/β-catenin pathway in eSZ cells and in Ewing's sarcoma cells. Gene set enrichment analyses (GSEA) using gene sets of *EWS-FLI1*–expressing eSZ and eGP cells 48 hours after gene introduction exhibited enrichment of genes within the WNT/β-catenin pathway as well as the EGF and RTK signaling pathways (Figure 6A and Supplemental Figure 7). In the